A Dual-ISM-Band Antenna of Small Size Using a Spiral Structure With Parasitic Element

J. L. Buckley, *Member, IEEE*, K. G. McCarthy, *Member, IEEE*, L. Loizou, *Member, IEEE*, B. O'Flynn, *Member, IEEE*, and C. O'Mathuna, *Fellow, IEEE*

***Abstract*—This letter presents a compact, single-feed, dual-band antenna covering both the 433-MHz and 2.45-GHz Industrial Scientific and Medical (ISM) bands. The antenna has small dimensions of 51×28 mm^2. A square-spiral resonant element is printed on the top layer for the 433-MHz band. The remaining space within the spiral is used to introduce an additional parasitic monopole element on the bottom layer that is resonant at 2.45 GHz. Measured results show that the antenna has a 10-dB return-loss bandwidth of 2 MHz at 433 MHz and 132 MHz at 2.45 GHz, respectively. The antenna has omnidirectional radiation characteristics with a peak realized gain (measured) of -11.5 dBi at 433 MHz and $+0.5$ dBi at 2.45 GHz, respectively.**

***Index Terms*—Antenna, compact, dual-band, inverted-F antenna (IFA), quality of service (QoS).**

I. Introduction

WIRELESS sensor network (WSN) technology is rapidly emerging in application areas such as smart healthcare and fitness monitoring. These systems are typically small, battery-powered devices operating in the 2.45-GHz ISM band using the IEEE 802.15.4 standard. However, the availability of other license-free bands such as the 433-MHz ISM band in Europe provides potential for quality-of-service (QoS) improvements. For example, the ability to adaptively switch from the 2.45-GHz to the 433-MHz ISM band can provide potential improvements such as reduced signal attenuation in biological monitoring applications as well as improved immunity to interference and congestion. Band switching can also offer improvements in data reliability, availability, and security when compared to existing solutions [1].

The requirement to switch between frequency bands poses a number of design challenges, however, because small, low-cost antenna structures with multiband capability are necessary. This area has been the subject of intense research in recent years with a large number of multiband antennas reported in the literature. These include a dual-band, inverted-F antenna (IFA) for 433/868 MHz [2], a printed-loop for 900/1800-MHz cellular applications [3], and a triple-band inverted-L topology for 2.4/5.2/5.8-GHz WLAN applications [4]. Other approaches use reconfigurable antennas where the antenna topology can be controlled electronically, for example using active RF switches [5]. Most passive, multiband antennas are generally resonant at a fundamental and a harmonic, or near harmonic, of the fundamental frequency. Only a limited number of small-sized, passive-type antennas are described in the literature that can cover both the lower and upper extents of the ISM bands, such as dual-band operation at 433 MHz and 2.45 GHz. Examples of small, multiband topologies are described in [6] and [7], but are designed for bio-implantable applications.

A small-sized antenna design is reported in [8] using a capacitively loaded IFA topology and a parasitic element to achieve dual-band operation at 930 MHz and 1.7 GHz. A conventional IFA requires a minimum size of $\lambda/4$, but this antenna is realized in a size of $0.109\lambda \times 0.025\lambda$, not including a ground plane. The design of electrically small antennas is challenging, however, as significantly decreasing the antenna size can adversely affect bandwidth, efficiency, and gain performance [9]. An electrically small antenna was recently reported by the authors covering the 433-MHz ISM band [10]. In this letter, we implement improvements to this antenna to allow coverage of the 2.45-GHz ISM band. The size of the original antenna is maintained at $0.07\lambda \times 0.05\lambda$ (at 433 MHz) including the ground plane.

This letter is organized as follows. Section II presents the proposed antenna topology. Section III describes antenna simulation and parametric analysis. Section IV presents the experimental results and discussion, and Section V concludes the letter.

II. Antenna Topology

Fig. 1 shows the configuration of the proposed dual-band antenna. The antenna structure is printed on a 1-oz, 1.524-mm, double-sided RO4350B laminate with a relative permittivity $\varepsilon_{\mathrm{R}} = 3.6$ and loss tangent $\tan\delta = 0.0031$. The total size of the antenna is 51×27.4 mm^2, and it is excited using a 50-Ω grounded-coplanar-waveguide (GCPW) feedline at Point A shown that is referenced to ground on both the top and bottom layers. A ground plane is printed on the bottom side of the substrate with dimensions of $W_{\mathrm{G}} \times L_1$, and the coplanar ground structures on the top side are connected to the ground plane using a series of through-hole vias as shown.

For the lower band (433 MHz), a square-spiral structure of width W_1 is printed on the top layer at the end of the feedline at Point B. This structure is a variation of an IFA topology with

Manuscript received April 30, 2015; revised June 22, 2015 and July 23, 2015; accepted August 04, 2015. Date of publication August 06, 2015; date of current version March 07, 2016. This work was supported by the EC SMArt Systems Co-design project (SMAC) FP7-ICT-2011-7-288827.

J. L. Buckley and B. O'Flynn are with the Tyndall National Institute, Cork, Ireland (e-mail: john.buckley@tyndall.ie; brendan.oflynn@tyndall.ie).

K. G. McCarthy is with the School of Engineering, Electrical and Electronic Engineering, University College Cork, Cork, Ireland (e-mail: k.mccarthy@ucc.ie).

L. Loizou was with the Tyndall National Institute, Cork, Ireland. He is now with Benetel Ltd., Dublin 8, Ireland (e-mail: loizos.loizou@ieee.org).

C. O'Mathúna is with the Tyndall National Institute, Cork, Ireland, and also with the Department of Electrical and Electronic Engineering, University College Cork, Cork, Ireland (e-mail: c.omatuna@tyndall.ie).

Color versions of one or more of the figures in this letter are available online at http://ieeexplore.ieee.org.

Digital Object Identifier 10.1109/LAWP.2015.2465831

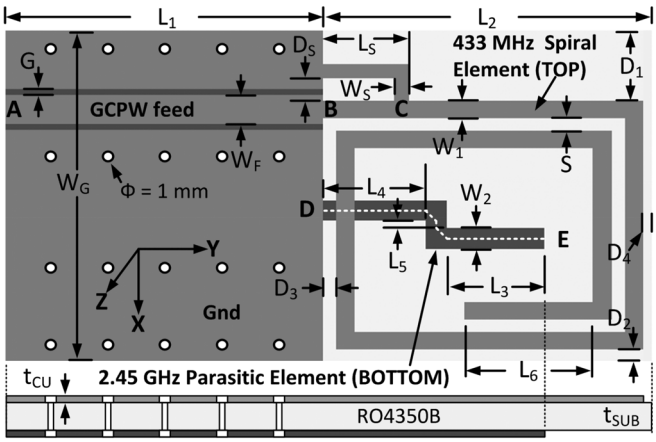

Fig. 1. Configuration of new dual-band 433-MHz/2.45-GHz antenna.

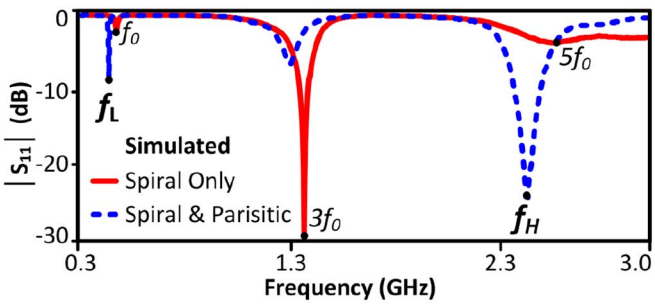

Fig. 2. Simulated return loss of antenna with and without parasitic element.

the spiral used to minimize the required area for this resonant section. At Point C, similar to an IFA configuration, a shunt inductive element is used to allow impedance matching of the antenna impedance to 50 Ω without the need for discrete matching components.

For the upper band (2.45 GHz), a parasitic monopole element is printed on the bottom layer at Point D with the element shorted to the ground plane as shown. This element has a width W_2 and a total length of $L_3+L_4+L_5+\sqrt{2}W_2$ as defined along the center of the element as shown. The monopole is staggered to maximize the monopole length and minimize the degree of end-coupling to the spiral at Point E.

III. Antenna Simulation

A. Antenna Resonant Behavior

The generalized resonant behavior of the antenna *with* and *without* the parasitic monopole element was first studied in simulation using a full-wave EM model of the antenna and solved using ANSYS HFSS [11]. Table I lists the parameters that were employed, except for L_6, L_3, and L_S that are specified here as $L_6 = 10$ mm, $L_3 = 5$ mm, and $L_S = 5$ mm and whose values were later optimized. Fig. 2 shows the simulated return loss from 300 MHz to 3 GHz. The multiband response of the antenna relates fundamentally to the intrinsic resonant properties of the spiral element that was designed to have a total electrical length of $\approx \lambda/4$ at $f_0 = 433$ MHz. The simulated response in Fig. 2 shows that with only the spiral element present, three distinct resonances are observed. The lowest resonance is shown at f_0, with two higher-frequency resonances observed at approximately odd multiples of f_0, i.e., $3f_0$ and $5f_0$. This behavior is characteristic of a $\lambda/4$ antenna structure that has harmonic

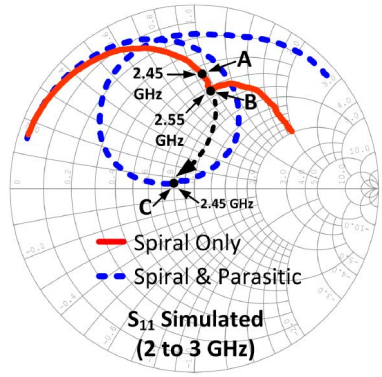

Fig. 3. Simulated S_{11} of the antenna with and without the parasitic element.

TABLE I
Optimized Design Parameters. All Dimensions Are in Millimeters

Name	Value	Name	Value	Name	Value	Name	Value
L_1	25.0	L_6	7.56	W_1	1.45	D_4	1.25
L_2	26.0	L_S	6.69	W_2	1.68	D_S	1.88
L_3	11.02	W_G	27.4	D_1	7.30	G	0.50
L_4	8.0	W_F	2.42	D_2	1.00	h	1.53
L_5	0.64	W_S	1.14	D_3	1.00	t_{CU}	0.035

resonances at odd multiples of the antenna's fundamental frequency [12]. The resonance at $3f_0$, or approximately 1.3 GHz, lies well outside both the ISM bands of interest and is therefore not considered further for this application. The resonances at f_0 and $5f_0$ are approximately 5% and 10% above the upper limits of the 433-MHz and 2.45-GHz ISM bands, respectively, but are not well matched to the 50-Ω source impedance. It can be seen from Fig. 2 that adding the parasitic element leads to a similar resonant response. However, in this case, with the monopole present, the three resonant frequencies occur at lower frequencies, and the impedance matching is greatly improved at the two frequencies of interest for this application (f_L and f_H).

In order to better understand this behavior, Fig. 3 plots the simulated antenna input impedance with and without the parasitic element present from 2 to 3 GHz. It can be seen that at Point A, with only the spiral element present, the antenna input impedance at 2.45 GHz is nonresonant or inductive. At Point B, a loop in the impedance profile is also observed at 2.55 GHz, corresponding to the return loss minimum at $5f_0$ in Fig. 2. When the parasitic monopole element is now introduced, a net capacitive loading effect is observed that results in a lowering of the resonant frequency from 2.55 to 2.45 GHz as well as enabling the antenna input impedance to be matched close to $50-\Omega$ at 2.45 GHz (shown graphically as the movement from Point B to Point C). In order to visualize the resonant modes of the antenna, the simulated surface current distributions are plotted in vector form in Fig. 4. It can be seen from Fig. 4(a) that a large current flows on the spiral element at 433 MHz, with very little current flow on the parasitic monopole element. Fig. 4(b) shows that at 2.45 GHz, the spiral has a second resonant mode, with 3 current maxima and 2 current minima present, indicating that the spiral has an electrical length of $\approx 5\lambda/4$ at 2.45 GHz. In this case, a large current flows on the parasitic element which has a resonant length of $\approx \lambda/4$ at 2.45 GHz and is excited via mutual coupling with the driven spiral element. Fig. 4(b) also shows that in-phase currents occur mainly on the horizontal sections of the spiral element with out-of-phase currents observed

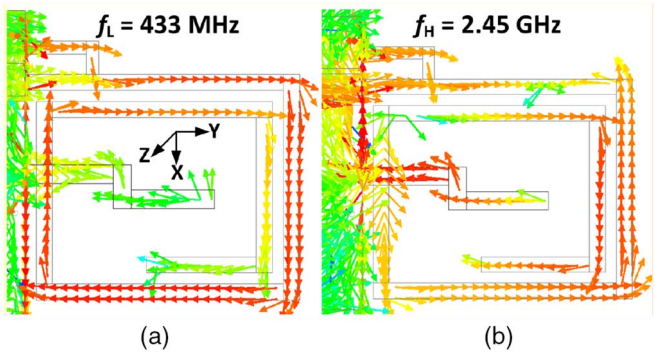

Fig. 4. Simulated antenna surface current distribution. (a) 433 MHz with $J_{SURF\_MAX} = 20$ A/m. (b) 2.45 GHz with $J_{SURF\_MAX} = 5$ A/m.

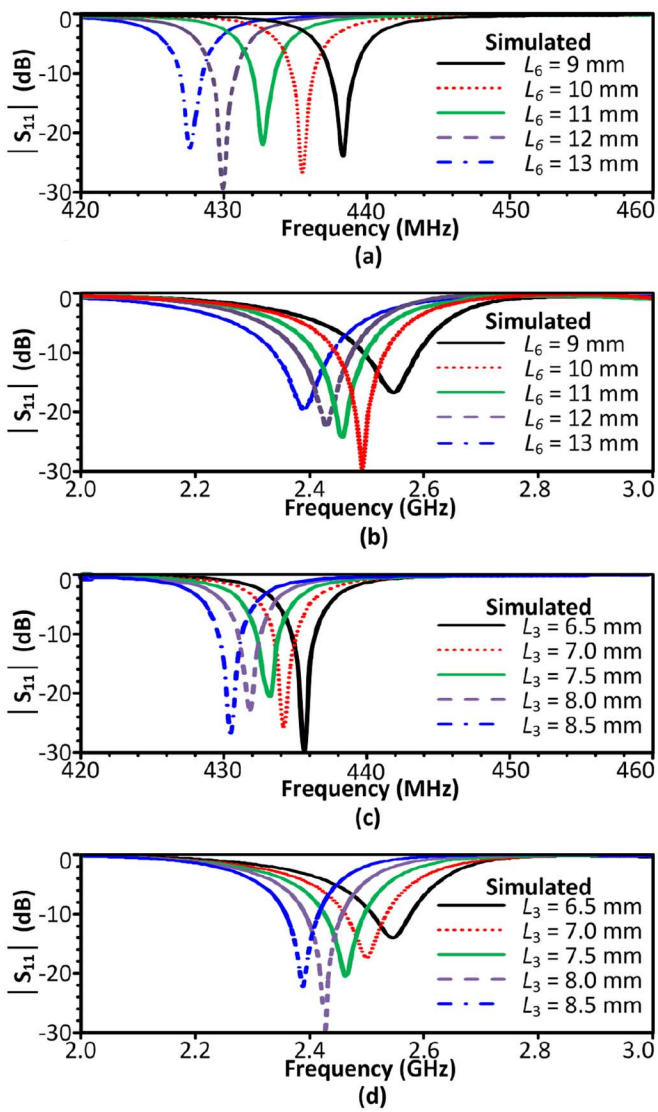

Fig. 5. Simulated $|S_{11}|$ for (a) varying L_6 low-band, (b) varying L_6 high-band, (c) varying L_3 low-band, (d) varying L_3 high-band.

largely on adjacent vertical sections. The combined radiation from the spiral and parasitic elements is therefore expected to be monopole-like, mainly due to the large currents flowing on the parasitic element at 2.45 GHz leading to enhanced radiation in the xz-plane with nulls present along the y-axis.

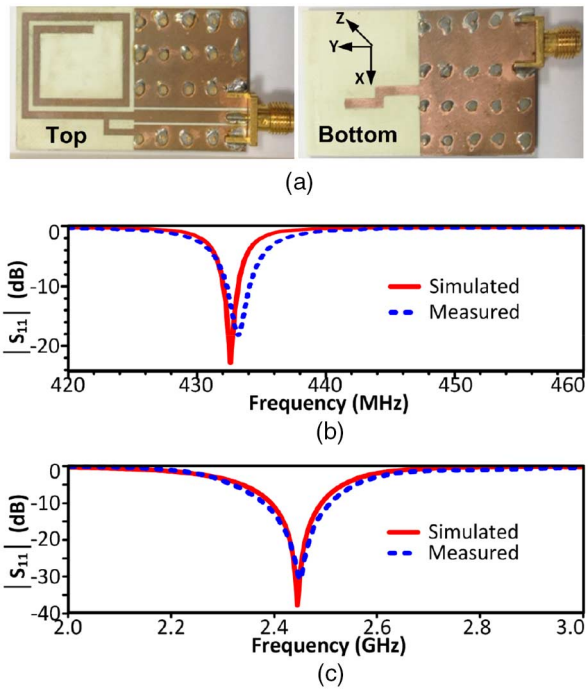

Fig. 6. (a) Photograph of prototype antenna showing top and bottom layers. (b) $|S_{11}|$ for the low band. (c) $|S_{11}|$ for the high band.

B. Parametric Analysis

In order to optimize the antenna for dual-band operation, the effects of several key parameters were investigated. Note that for subsequent discussion and presentation of results, only the lower and upper band responses are considered and for clarity are plotted separately. The influence of the spiral length on the lower and upper bands was first studied. The spiral end-length L_6 was varied while keeping all other parameters constant according to the values listed in Table I. Fig. 5(a) and (b) show that the resonant frequencies for both the low and high bands decreases with increasing L_6, and the impedance matching for the upper band, in particular, is also affected. The influence of the monopole end-length parameter L_3 is summarized in Fig. 5(c) and (d). It can be seen that the resonant frequencies for both the lower and upper bands are also seen to decrease for increasing L_3 and the impedance matching for both bands is also affected, particularly for the upper band. The mutual coupling between the spiral and parasitic element accounts for the observed effects as lengthening either element leads to a decrease in resonant frequencies for both bands. The effects of varying the shunt inductance length L_S were also investigated but are not plotted here. It was determined that parameter L_S allows a good degree of independent control of the impedance matching for the lower band with a small effect on the resonant frequency for both bands but primarily for the low band. The above parametric simulations show that frequencies f_L and f_H are primarily determined by the total length of the spiral element. The results of Fig. 5 also show that a sufficient degree of independent control is possible using parameters L_3, L_6, and L_S to enable the lower and upper frequency bands to be tuned and matched over the frequency range shown. The optimized antenna design parameters are listed in Table I.

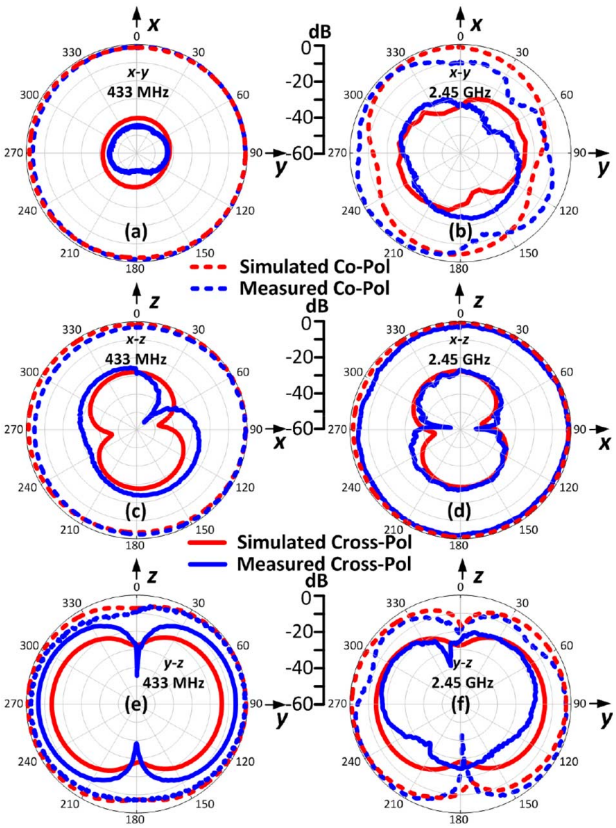

Fig. 7. Measured and simulated radiation patterns: (a) xy-plane at 433 MHz, (b) xy-plane at 2.45 GHz, (c) xz- plane at 433 MHz, (d) xz-plane at 2.45 GHz, (e) yz-plane at 433 MHz, (f) yz-plane at 2.45 GHz.

IV. Results and Discussion

In order to verify the proposed design, a prototype antenna was developed as shown in Fig. 6(a) using an LPKF ProtoMat C60 milling machine. The top and bottom ground interconnections were made using brass pins as shown. The impedance and radiation characteristics of the antenna were then measured in an anechoic chamber using a Vector Network Analyzer. In order to suppress cable current effects, the measurements were performed using a balun and ferrite-beaded cable [2]. The return loss plots of Fig. 6(b) and (c) show the dual-band nature of the antenna, and the measured and simulated results show good agreement. The small discrepancies in resonant frequency are most likely attributed to fabrication tolerances for the prototype. The antenna has a measured 10-dB return-loss bandwidth of 2 MHz at 433 MHz, and 132 MHz at 2.45 GHz, that are sufficient to cover the 1.75-MHz and 80-MHz bandwidth requirements.

The measured and simulated radiation patterns for the principal planes are shown in Fig. 7. Overall, the antenna exhibits desirable omnidirectional characteristics for both bands, and good agreement between measured and simulated results is observed, especially for the xz-plane. The differences between the measured and simulated results for the xy- and xz-planes are attributed to the effects of adding a 90° adapter during these measurements. The addition of the adapter has the effect of moving the axis of measurement away from the phase-center of the antenna when measuring the xy- and xz-patterns. In addition, the adapter increases the possibility for coupling between the antenna and the ferrite absorber material and balun, especially for the 2.45-GHz band. Both of the above effects can lead to perturbation of the radiation pattern in the measurement setup, and these effects are not modeled in simulation. It can also be observed from Fig. 7 that the radiation nulls predicted from the current distribution of Fig. 4 are also evident in the measurements.

The peak realized gain was measured as -11.5 dBi at 433 MHz and $+0.5$ dBi at 2.45 GHz with the maximum gain measured in the xz-plane for both frequency bands. The measured gain figures compare well to the simulated values (-10.25 dBi at 433 MHz and 1.45 dBi at 2.45 GHz), and it can be seen that band switching allows adaptive control of antenna gain to suit the link requirements of the application. The antenna has a simulated radiation efficiency of approximately 7% at 433 MHz and 72% at 2.45 GHz. The relatively low gain and radiation efficiency figures at 433 MHz are expected since the antenna is electrically small [9] but these effects are offset to a large degree by significantly reduced path loss ($\sim$ 15 dB) at 433 MHz when compared to 2.45 GHz.

V. Conclusion

In this letter, a compact, single-feed planar antenna that operates in both the 433-MHz and 2.45-GHz ISM bands has been proposed and implemented. Dual-band operation is achieved using a spiral element and a parasitically coupled monopole element. The antenna is realized in a small size of $0.07\lambda \times 0.05\lambda$ at 433 MHz including the ground plane. The antenna is linearly polarized with desirable omnidirectional radiation characteristics. The ability of the antenna to cover both the lower and upper extents of the UHF ISM bands together with its small physical size and cost make it suitable for a wide variety of short-range, wireless applications.

References

[1] E. Popovici *et al.*, "The s-Mote: A versatile heterogeneous multi-radio platform for wireless sensor networks applications," in *Proc. 20th ECCTD*, 2011, pp. 421–424.

[2] L. Loizou, J. Buckley, and B. O'Flynn, "Design and analysis of a dual-band inverted-F antenna with orthogonal frequency-controlled radiation planes," *IEEE Trans. Antennas Propag.*, vol. 61, no. 8, pp. 3946–3951, Aug. 2013.

[3] C. Yun-Wen and W. Kin-Lu, "Internal compact dual-band printed loop antenna for mobile phone application," *IEEE Trans. Antennas Propag.*, vol. 55, no. 5, pp. 1457–1462, May 2007.

[4] J. Jen-Yea and T. Liang-Chih, "Small planar monopole antenna with a shorted parasitic inverted-L wire for wireless communications in the 2.4-, 5.2-, and 5.8-GHz bands," *IEEE Trans. Antennas Propag.*, vol. 52, no. 7, pp. 1903–1905, Jul. 2004.

[5] M. Fallahpour, M. T. Ghasr, and R. Zoughi, "Miniaturized reconfigurable multiband antenna for multiradio wireless communication," *IEEE Trans. Antennas Propag.*, vol. 62, no. 12, pp. 6049–6059, Dec. 2014.

[6] R. S. Alrawashdeh, Y. Huang, M. Kod, and A. A. B. Sajak, "A broadband flexible implantable loop antenna with complementary split ring resonators," *IEEE Antennas Wireless Propag. Lett.*, vol. 14, pp. 1322–1325, 2015.

[7] X. Li-Jie, G. Yong-Xin, and W. Wen, "Dual-band implantable antenna with open-end slots on ground," *IEEE Antennas Wireless Propag. Lett.*, vol. 11, pp. 1564–1567, 2012.

[8] K. Jae Hee, C. Won Woo, and P. Wee Sang, "A small dual-band inverted-F antenna with a twisted line," *IEEE Antennas Wireless Propag. Lett.*, vol. 8, pp. 307–310, 2009.

[9] H. A. Wheeler, "Fundamental limitations of small antennas," *Proc. IRE*, vol. 35, no. 12, pp. 1479–1484, Dec. 1947.

[10] J. Buckley *et al.*, "Compact 433 MHz antenna for wireless smart system applications," *Electron. Lett.*, vol. 50, pp. 572–574, 2014.

[11] ANSYS HFSS. ANSYS, Jan. 2015 [Online]. Available: http://www.ansys.com

[12] J. D. Kraus, *Antennas for All Applications*, 3rd ed. New York, NY, USA: McGraw-Hill, 2002, pp. 181–183.